Published in final edited form as:
Phys Med Biol. 2014 June 7; 59(11): 2813–2828. doi:10.1088/0031-9155/59/11/2813.

Simultaneous Tc-99m/I-123 Dual Radionuclide Myocardial Perfusion/Innervation Imaging Using Siemens IQ-SPECT with SMARTZOOM Collimator

Yong Du[1], **Manojeet Bhattacharya**[2], and **Eric. C. Frey**[1]

[1]Department of Radiology, Johns Hopkins University, 601 N Caroline Street, JOHC 4263, Baltimore, MD 21287, USA

[2]Molecular Imaging Science and Technology, Siemens Medical Solutions USA Inc., 2501 N. Barrington Road, Hoffman Estates, IL 60192, USA

Abstract

Simultaneous dual-radionuclide myocardial perfusion/innervation SPECT imaging can provide important information about mismatch between scar tissue and denervated regions. The Siemens IQ-SPECT system developed for cardiac imaging uses a multifocal SMARTZOOM collimator to achieve a four-fold sensitivity for the cardiac region compared to a typical parallel-hole low-energy high-resolution collimator but without the data truncation that can result with conventional converging-beam collimators. The increased sensitivity allows shorter image acquisition times or reduced patient dose, making IQ-SPECT ideal for simultaneous dual-radionuclide SPECT, where reduced administrated activity is desirable in order to reduce patient radiation exposure. However, crosstalk is a major factor affecting the image quality in dual-radionuclide imaging. In this work we developed a model-based method that can estimate and compensate for the crosstalk in IQ-SPECT data. The crosstalk model takes into account interactions in the object and collimator-detector system. Scatter in the object was modeled using the effective source scatter estimation technique (ESSE), previously developed to model scatter with parallel-hole collimators. The geometric collimator detector response was analytically modeled in the IQ-SPECT projector. The estimated crosstalk was then compensated for in an iterative reconstruction process. The new method was validated with data from both Monte Carlo simulation and physical phantom experiments. The results showed that the estimated crosstalk was in good agreement with simulated and measured results. After model-based compensation the images from simultaneous dual-radionuclide acquisitions were similar in quality to those from single radionuclide acquisitions that did not have crosstalk contamination. The proposed model-based method can be used to improve simultaneous dual-radionuclide images acquired using IQ-SPECT. This work also demonstrates that ESSE scatter modeling can be applied to non-parallel-beam projection geometries.

Keywords

simultaneous dual-radionuclide SPECT; myocardial perfusion; myocardial innervation

Introduction

SPECT imaging is an important tool for diagnosing cardiac diseases. Myocardial perfusion SPECT images acquired using a ^{99m}Tc labeled agent, such as ^{99m}Tc sestamibi or ^{99m}Tc tetrofosmin (Zaret and Beller, 2010b), are commonly used to detect cardiovascular diseases, helping identify location and level of stenosis or infarction, and assessing viability of infarcted myocardium. The use of myocardial innervation imaging with ^{123}I MIBG has been increasing, especially for studying patients after myocardial infarction or with congestive heart failure (Zaret and Beller, 2010a; Miyamoto *et al.*, 1999; Pace *et al.*, 2004; Raffel and Wieland, 2010; Sakata *et al.*, 2009). In these diseases, the sympathetic nerves controlling myocardial function can be damaged, reducing cardiac innervation density, referred to as denervation. A denervated region that is larger than the infarct can lead to arrhythmia and ventricular fibrillation, and potentially to sudden cardiac death. Therefore it is very important to find regions of mismatch between infarcted myocardium and denervated region in order to provide appropriate medical or surgical intervention (Zhao *et al.*, 2001; Yukinaka *et al.*, 1998; Agostini *et al.*, 2002).

One way to find the mismatch is to compare the perfusion images with the innervation images. Because the two images are acquired with radiopharmaceuticals labeled with different radionuclides, i.e., ^{99m}Tc and ^{123}I, the perfusion images and the innervation images can be acquired using the dual-radionuclide simultaneous acquisition imaging techniques (Du and Frey, 2007; Buvat *et al.*, 1999; Devous *et al.*, 1992; El Fakhri *et al.*, 2000; Ivanovic *et al.*, 1994; Moore *et al.*, 1995; Ouyang *et al.*, 2007; de Jong *et al.*, 2002). Using the ability of modern SPECT systems to acquire data in multiple energy windows, in simultaneous dual-radionuclide imaging, projection images of the two radiopharmaceutical distributions can be acquired at the same time. This will reduce the total imaging time, improve patient comfort, and perhaps most important, provide images perfectly registered in both space and time that are ideal for detecting, both visually and quantitatively, mismatch between infarcted and denervated regions.

However, in simultaneous dual-radionuclide imaging gamma photons emitted by one radionuclide can be detected in another radionuclide's energy window, referred to as crosstalk contamination. The crosstalk is caused by both photon interactions inside the patient body and photon interactions with the collimator-detector system. In these interactions, Compton scattering can reduce a photon's energy and result in it being detected in another radionuclide's energy window (downscatter). The limited energy resolution of SPECT systems and the proximity of the two photopeaks also results in photons emitted from one radionuclide being detected in another radionuclide's energy window, causing contamination. If not compensated for, the crosstalk can cause artifacts and significantly reduce image quality of the simultaneously acquired images.

Another important concern with dual-radionuclide imaging is the potentially large patient radiation dose resulting from using two radiopharmaceuticals. To improve image quality and reduce patient dose, innovations in both image reconstruction and compensation methods and the imaging hardware are required. We have previously developed model-based methods that can accurately estimate and compensate for the crosstalk contamination in simultaneous dual-radionuclide imaging. The methods have been successfully applied and validated in ^{99m}Tc/^{20l}Tl cardiac rest/stress perfusion imaging and ^{99m}Tc/^{123}I brain imaging, etc (Song *et al.*, 2004; Kadrmas *et al.*, 1999; Du and Frey, 2007, 2009; Du *et al.*, 2007; He *et al.*, 2008; Du *et al.*, 2014).

Siemens has developed the IQ-SPECT system for cardiac imaging that uses a multifocal SMARTZOOM collimator (Rajaram *et al.*, 2011; Pirich *et al.*, 2012). The holes of a SMARTZOOM collimator are focusing in nature at the center, to improve sensitivity for the cardiac region, and near-parallel at the edge, to allow acquisition of untruncated projection data. By aiming the center of the collimator at the heart during acquisition, this system can achieve a four-fold sensitivity for the cardiac region compared to a low-energy high-resolution (LEHR) parallel-hole collimator (Rajaram *et al.*, 2011). The increased sensitivity allows shorter image acquisition time, reduced patient dose, or a combination of both. This makes IQ-SPECT ideal for acquiring simultaneous dual-radionuclide SPECT by enabling reduced administered dose without increasing image noise.

To take advantage of both model-based compensation and IQ-SPECT, in this work, we adapted the model-based crosstalk estimation and compensation method to IQ-SPECT for simultaneous ^{99m}Tc/^{123}I dual-radionuclide myocardial perfusion/innervation imaging. We first developed and validated a fast Monte Carlo simulation method for simulating the image formation process of IQ-SPECT. Then we adapted the model-based method to IQ-SPECT. The method was then validated with data from both Monte Carlo simulation and physical phantom experiments.

Methods

Fast Monte Carlo Simulation of IQ-SPECT

Monte Carlo simulation is very useful for validating crosstalk estimation and compensation. Due to its multifocal nature, it is difficult to model the SMARTZOOM collimator using existing Monte Carlo simulation methods. Therefore, a fast Monte Carlo simulation method was first developed to model the IQ-SPECT with SMARTZOOM collimator. A previously developed Angular Response Function (ARF) method for parallel-hole collimator (Song *et al.*, 2005) was modified to use a vector map that contains direction information about each collimator hole in the SMARTZOOM collimator and the real time orbit information to correctly model the photon interactions with the SMARTZOOM collimator. In the method, photon interactions with the collimator-detector system, including geometrically collimated photons and photons penetrating through and scattered in the collimator septa, were modeled using pre-calculated ARF tables. The ARF tables contain the probabilities of detecting incident photons as a function of the angles between the collimator hole axis and the photon propagation direction. Because the SMARTZOOM collimator is a multifocal collimator with varying focal length, the ARF tables were computed based on Monte Carlo simulation

of point sources in front of a parallel-hole collimator that models an average SMARTZOOM collimator hole geometry.

During the ARF simulation, the photon interaction inside the object was first modeled using SimSET and saved to a history file (R. L. Harrison, 1993; R. L. Harrison, 1994). When a photon exited the object and reached the collimator, the incident angle between the photon and the SMARTZOOM collimator hole at the incident location was computed based on the vector map and orbit information of that specific collimator and projection view. This angle of incidence was used to select the appropriate detection probability from the ARF tables. The intersection of the photon direction with the detection plane was computed and the detection probability was summed into the projection bin containing this intersection position. This process was repeated for a large number of photons; summing the detection probabilities of all the photons gave the final projection data.

The modified ARF method was validated with two physical phantom experiments. The first experiment validated the projection geometry, response, and sensitivity of the simulation. Three 4 ml spheres in air aligned in a diagonal direction in front of an IQ-SPECT camera were used. The spheres were 15 cm apart and contained the same ^{99m}Tc activity concentration. The sphere in the center was 28 cm from the face of collimator. The projections at planes parallel and perpendicular to the 3 spheres were acquired in a 15% ^{99m}Tc energy window and 128 by 128 projection bins with a bin size of 0.4795 cm. The ARF simulation modeled exactly the same setup. A total of 50 million photons were simulated.

Figure 1 shows the phantom setup in the second experiment that validated accuracy of the simulation in terms of attenuation, scatter, and collimator-detector response. Three spheres filled with a 0.45 mCi/cc ^{99m}Tc activity concentration were placed in a water filled cylindrical phantom (diameter 22 cm). The volumes of the spheres, from left to right, were 12.6 ml, 12.6 ml and 5.6 ml, respectively. The phantom was placed on the imaging table with the middle sphere centered in the field of view. Projections were acquired using a typical IQ-SPECT cardiac imaging protocol: 128 by 128 projection matrix with a bin size of 0.4795 cm; 28 cm radius of rotation; 34 views from right anterior oblique view to left posterior oblique view. To acquire low noise data, 60 seconds per view imaging time was used. The same phantom and camera setup was also used in the SimSET-ARF Monte Carlo simulation to generate full IQ-SPECT projections. A total of 300 million photons were simulated, taking 4 hours to complete on a computer with an AMD Opteron 275 2.2 GHz CPU and 2 GB memory.

Model-Based Crosstalk Estimation and Compensation

To model the crosstalk from ^{123}I into the ^{99m}Tc energy window, photons were separated into groups based on their interactions. The first group was the photons that were scattered in the object and detected in the ^{99m}Tc energy window after being geometrically collimated by the SMARTZOOM collimator. Photon interactions with the crystal, including backscatter from material behind crystal, were also included. The scatter was modeled using the effective source scatter estimation technique (ESSE) (Frey and Tsui, 1997), where an effective scatter source was first calculated for each projection view by convolving the

estimated ^{123}I activity image with the object independent scatter kernels followed by multiplication with an electron density map derived from the attenuation map. The effective scatter source was then attenuated and projected with modeling of the collimator hole geometry and the effects of varying focal lengths of the multifocal SMARTZOOM collimator to form an estimate of the scatter in the IQ-SPECT projection data.

The scatter kernels represent probabilities of photons emitted from a point source that are scattered into 3-dimensional space. In this work, they were calculated by Monte Carlo simulation of all ^{123}I photons, including 159 keV and high-energy photons, detected in the ^{99m}Tc window using an ideal parallel hole collimator. The use of the parallel-hole geometry to generate the effective scatter source is an approximation with the assumption that the cross section at the last scatter point and energy after scattering calculated for the parallel hole can be used to describe the scatter for SMARTZOOM geometry. This approximation allows efficient estimation of the effective scatter source using convolution, with the SMARTZOOM collimator the relationship between the last scatter point and the scatter angle required to pass through a collimator hole is spatially varying. As shown in the results, this approximation did not affect the accuracy of crosstalk estimation due to slow variation of the scatter distribution as a function of scatter angle.

The unscattered ^{123}I 159 keV photons that were detected in the ^{99m}Tc energy window were also modeled. The detection of these photons resulted mainly from the limited energy resolution and was modeled by scaling the ^{123}I projections in its own energy window with a factor computed from a Gaussian energy resolution model. Similarly, the crosstalk from ^{99m}Tc photons into the ^{123}I energy windows was mainly due to the detection of unscattered 140.5 keV photons counted in the ^{123}I energy window due to the finite energy resolution, and was modeled in the same way.

Some of the scattered and unscattered ^{123}I high-energy photons can penetrate or scatter in the collimator septa and are then detected in the ^{99m}Tc energy window. These photons were not modeled because the IQ-SPECT SMARTZOOM collimator has long holes and thick septa that are close to those of a medium energy collimator. The amount of septal penetration and scatter, therefore, is small as compared to imaging with a low-energy high-resolution collimator.

To compensate for the crosstalk contamination, both ^{123}I and ^{99m}Tc images were first reconstructed without crosstalk compensation. The reconstructed images were then used to estimate the crosstalk with the model-based method. The crosstalk was then compensated for during a second iterative reconstruction process by adding the estimated crosstalk to the estimated projection data. Compensation could also be accomplished by directly subtracting the estimated crosstalk from projection data.

Monte Carlo Simulation Validation

The model-based crosstalk compensation method (MBC) was first validated using a Monte Carlo simulation study. The XCAT phantom was used to generate realistic digital phantoms that modeled ^{99m}Tc tetrofosmin and ^{123}I MIBG uptake in a patient (Fung *et al.*, 2011). The activity concentrations and concentration ratios between ^{99m}Tc and ^{123}I in each organ are

shown in Table 1. A lateral wall-mid ventricular myocardial defect was also simulated for each radionuclide. For ^{99m}Tc, the defect was 3 cm along the long axis and spanned 90° around the short axis. For ^{123}I, the defect was 3 cm long and had an angular range of 180°. The uptake in the defect is also shown in Table 1.

The IQ-SPECT projections of the phantom were simulated using the newly developed SimSET-ARF method. The simulated projection bins were 128 by 128 with a bin size of 0.4795 cm. The radius of rotation was 28 cm. A total of 34 views from 45° right anterior oblique to 45° left posterior oblique were generated. A total of 8 billion photons were simulated for each radionuclide. The simulation would have taken a total of 80 hours on a computer with an AMD Opteron 275 2.2 GHz CPU and 2 GB memory, but was actually much faster on our computer cluster with multiple cores. The 159 keV ^{123}I photons and 140.5 keV ^{99m}Tc photons were simulated separately to generate projections in both the ^{123}I and ^{99m}Tc photopeak energy windows. The ^{123}I high-energy photons were not included in the simulation because the amount of septal penetration and scatter was assumed small for the SMARTZOOM collimator. After simulation, projections from both radionuclides were summed to generate simultaneous dual-radionuclide data. The resulting activity concentration ratios between ^{99m}Tc and ^{123}I in each organ are also given in Table 1.

The simulated projection data were reconstructed using the OS-EM algorithm with 20 iterations and 2 subsets per iteration. The two subsets per iteration were used because there are only 34 projection views acquired using a standard IQ-SPECT protocol. Thus one must use either 2 or 17 subsets per iteration or use subsets with unequal numbers of projection views. Using 17 subsets may result in a noise or convergence problems, so we chose to reconstruct images with 2 subsets per iteration and 20 iterations. The 20 iterations were chosen because the log likelihood converged after this number of iterations. Compensations for attenuation and the geometric collimator-detector response were included in the reconstruction. The model-based method was applied to compensate for the crosstalk in both ^{123}I and ^{99m}Tc images. For comparison, single-radionuclide images without crosstalk contamination were also reconstructed with the same parameters. The scatter of photopeak photons into their own energy window was not compensated for in either the single-radionuclide images or the dual-radionuclide images. This was done because in clinical protocols scatter is not commonly compensated for. Please note the model-based method can be used to estimate and compensate for the scatter of photopeak photons into its own energy window if required.

Physical Phantom Experiment Validation

Physical phantom experimental data were acquired using a Data Spectrum Torso phantom on a Siemens Symbia SPECT/CT system. The ^{99m}Tc and ^{123}I activity were imaged separately, allowing us to sum the data to generate simultaneous dual-radionuclide projections while still providing separately acquired single radionuclide data as truth for evaluation. The phantom was first filled with ^{123}I activities to mimic an MIBG uptake ratio typical of a patient study (Table 2). No activity was placed in the lungs. Two transmural cardiac defects with zero activity were placed at the anterior and inferior walls at a mid-ventricular position. The defect sizes were 2 cm along the long axis and 45°

circumferentially. Projection data were then acquired simultaneously using a 149–171 keV ^{123}I energy window and a 131–149 keV ^{99m}Tc energy window with a typical IQ-SPECT acquisition protocol of 34 projections from right anterior oblique to left posterior oblique. The heart was centered in the field of view for maximum sensitivity. The projection matrix size was 128 by 128 pixels with 0.4795 cm pixels. The radius of rotation was 28 cm. The imaging duration was 15 s per view. A CT scan of the phantom was performed after SPECT acquisition with default settings to generate attenuation maps. After ^{123}I activities decayed to the background level, the phantom was cleaned and filled with ^{99m}Tc to mimic a typical patient ^{99m}Tc tetrofosmin activity distribution (Table 2). A single transmural cardiac defect with zero activity and the same size as above was placed in the septal wall at a mid-ventricular position. The phantom was then carefully placed back on the imaging table to match the position used in the ^{123}I study. IQ-SPECT data and CT images were then acquired using same parameters listed above.

Simultaneous dual-radionuclide projection data were generated by summing the single-radionuclide projections in the corresponding energy windows. The activity concentration ratios of ^{99m}Tc and ^{123}I are also listed in Table 2. The same reconstruction and compensation procedures used in the simulation validation above were also used here. Single-radionuclide images without crosstalk contamination were also reconstructed as gold standards.

Results

SimSET-ARF Monte Carlo Simulation

Figure 2 compares SimSET-ARF simulated and experimentally acquired results of three identical spheres in air. Projections acquired from views both parallel and perpendicular to the plane containing the sphere are shown. Profiles passing through centers of the spheres are plotted below the images in Figure 2. There was very good agreement between the simulated and experimentally measured results, indicating that simulation using the SimSET-ARF method can accurately model the SMARTZOOM collimator. Figure 2 also demonstrates that the point spread function of the SMARZOOM collimator is spatially shift-variant, and the center region has a much higher sensitivity then the peripheral regions. Please note that the dark area in the experimental projection in Figure 2b was due to attenuation from a plastic plate that held the spheres, which was not modeled in the simulation.

Figure 3 compares SimSET-ARF simulated and experimentally acquired projections of three spheres in a water filled cylinder from several views. Horizontal profiles through the centers of three spheres are plotted in Figure 4 for the first and the forth projections in the Figure 3. There was very good agreement between the simulation and experiment. The profiles are almost identical to each other on both linear and logarithmic vertical scales, demonstrating that both unscattered photons and the photons scattered inside the object were correctly simulated using the SimSET-ARF method. These data suggest that the SimSET-ARF method can be used to accurately simulate the IQ-SPECT cardiac imaging to validate the model-based crosstalk compensation method in the following studies.

Monte Carlo Simulation Validation of Model-Based Method

In Figure 5, the estimated crosstalk from ^{123}I into the ^{99m}Tc energy window is compared with simulated results for an anterior projection view. The horizontal profiles across the heart region are also plotted in Figure 5. Contributions from unscattered photons (primary) and photons scattered inside the object (scatter) are shown separately in addition to the total crosstalk, which is the sum of the two. There was good agreement between the model-based estimates of the crosstalk and the SimSET-ARF simulated results for primary photons, scattered photons, and the total crosstalk. The figure also shows that most of crosstalk form ^{123}I into the ^{99m}Tc energy window was due to downscatter of ^{123}I photons with reduced energies that is detectable in the ^{99m}Tc energy window. Overall, the downscatter accounted for about 90% of the total crosstalk. The contribution from unscattered primary photons due to energy resolution was only 10% of the total crosstalk.

Comparison of estimated crosstalk from ^{99m}Tc into the ^{123}I energy window is shown in Figure 6. Horizontal profiles across the heart region were also plotted in Figure 6. Please note only contributions from unscattered ^{99m}Tc primary photons are included. Both the projection images and the profiles are in good agreement with the simulated results, indicating the accuracy of the model-based method.

Figure 7 shows short axis images and circumferential profiles of both ^{123}I and ^{99m}Tc with and without model-based crosstalk compensation. Single-radionuclide images without crosstalk contamination were also included. Circumferential profiles were calculated by averaging the counts inside a 4 pixel-wide ring from endocardium to epicardium of the three adjacent short axis slices in Figure 7, which had the most severe defect. The crosstalk from ^{99m}Tc into the ^{123}I energy window was mainly from unscattered photons, and its effects on the ^{123}I images were local. As shown in Figure 7a, intensities in the anterior, septal, and inferior wall were increased by crosstalk from ^{99m}Tc in these regions with normal ^{99m}Tc uptake. On the other hand, the ^{99m}Tc uptake in the lateral wall was much lower due to the ^{99m}Tc defect, resulting in a negligible amount of crosstalk to the ^{123}I energy window in that region. Therefore the lateral wall in ^{123}I images was almost unchanged with or without crosstalk contamination. This resulted in a spurious increase in defect contrast of the ^{123}I images without crosstalk compensation, reducing the defect to normal activity concentration ratio to 0.567. After model-based compensation, the crosstalk was largely removed and the profiles were almost identical to those of the single-radionuclide images. The defect to normal activity concentration was increased to 0.589, which was close to the value of 0.591 from the single-radionuclide ^{123}I images. These values were higher than the true value of 0.3. This was likely due to a combination of factors that were not compensated for in this study, including scattered 159 keV ^{123}I photons detected in the ^{123}I photopeak energy window and partial volume effects. All these factors would tend to reduce image contrast, in the ^{123}I image, resulting in an increased defect to normal ratio.

Most of the crosstalk from ^{123}I into the ^{99m}Tc energy window was downscatter with a broad and flat spatial distribution, raising the overall intensity of the ^{99m}Tc images. As shown in Figure 7b, the profiles of the ^{99m}Tc image without crosstalk compensation were higher than the single-radionuclide images, potentially reducing the defect contrast. After model-based

crosstalk compensation, the effects of crosstalk contamination were removed and the profiles were almost identical with the single-radionuclide images. The defect to normal activity concentration ratio was also calculated from circumferential profiles. The value in the dual-radionuclide ^{99m}Tc images was 0.328 without crosstalk compensation. After model-based compensation, the defect to normal activity concentration ratio improved to 0.267, which was close to the ratio of 0.274 in the single-radionuclide ^{99m}Tc images.

Physical Phantom Experiment Validation of Model-Based Compensation Method

Figure 8 shows the model-based crosstalk estimates compared with measured crosstalk for a right anterior oblique view. Horizontal profiles across the heart region are also plotted in Figure 8. For this experiment, the total crosstalk contamination in the ^{99m}Tc energy window was 17.5% of the total counts; the total crosstalk contamination in the ^{123}I energy window was 10.9% of the total counts. Again, there was very good agreement between the model-based crosstalk estimates and the measured crosstalk. The small disagreement in the tail region outside the object in Figure 8a could be due to the high-energy ^{123}I photons that penetrated or scattered in the collimator septa, which were not modeled. However their contribution was very small as shown in the figure. Explicitly modeling these photons would require modeling them in the IQ-SPECT SMARTZOOM projector.

Figure 9 shows short axis dual-radionuclide ^{123}I images and their circumferential profiles with and without model-based crosstalk compensation. Single-radionuclide ^{123}I images without crosstalk contamination are also shown. The profiles were calculated the same way as described in the simulation validation. The two defects located in the anterior and inferior walls can be seen clearly. Crosstalk from ^{99m}Tc photons created an artifactual defect in the inferior-septal region as indicated by the arrows. The overall profiles were also raised by the crosstalk. After model-based compensation, the artifactual defect was removed and the entire profile agreed well with that from the single-radionuclide images. The defect to normal activity concentration ratio computed from the circumferential profiles was 0.675 without crosstalk compensation, and 0.691 after model-based compensation, which was close to the ratio of 0.699 from the single-radionuclide ^{123}I images.

Figure 10 shows reconstructed short axis ^{99m}Tc images and their circumferential profiles. Again, without compensation the crosstalk raised the entire profile and reduced defect contrast in the ^{99m}Tc image. The defect to normal activity concentration ratio was 0.268 without compensation. After model-based compensation, the images were close to the single-radionuclide images with almost identical profiles. The defect to normal activity concentration ratio was reduced to 0.211 and was close to the value of 0.200 from the single-radionuclide images, demonstrating improved fidelity of the defect contrast.

Discussion

^{123}I MIBG cardiac innervation imaging has received recent interest for applications in cardiac imaging, especially since the recent approval by the FDA for heart failure indications. Combining ^{123}I MIBG innervation images and myocardial perfusion images to find mismatch between infarcted scar tissue and denervated region is potentially important to identify patients at risk for developing ventricular fibrillation or tachycardia and

identifying candidate regions for ablative therapies. Untreated, those conditions could lead to sudden cardiac death, the source of over 335,000 fatalities per year in the U.S alone. Therefore it is important to identify those patients for treatment and intervention. Simultaneous dual-radionuclide ^{123}I MIBG and ^{99m}Tc sestamibi/tetrofosmin perfusion imaging seems to be an ideal fit for this purpose, providing perfectly registered images to identify the mismatch between perfusion and innervation. However, there are technical challenges that could limit its clinical utility including crosstalk and patient radiation dose concerns.

Previously there has been substantial effort to develop methods that can estimate and compensate for the crosstalk contamination. Recently, several new camera systems based on semiconductor detectors have also been developed for cardiac imaging (Schillaci and Danieli, 2010). Due to the higher energy resolution of the semiconductor detectors used in these cameras, these systems could provide simultaneous dual-radionuclide images with less crosstalk contamination (Ben-Haim *et al.*, 2010; Milliner *et al.*, 2012). However, they are usually quite expensive and dedicated cardiac systems may be difficult to justify in some clinical environments. In addition, as shown in Figure 5, a substantial fraction of crosstalk from ^{123}I into the ^{99m}Tc window is photons that scatter in the patient or collimator and are detected in the ^{99m}Tc window. Even with increased energy resolution this contamination will still be present.

The IQ-SPECT system uses a multi-focal collimator (named SMARTZOOM) on a conventional camera system to increase the sensitivity. This increased sensitivity could be traded for reduced patient dose, providing a lower cost alternative to semiconductor detector based systems. In this work we have shown that previously-developed model-based crosstalk estimation and compensation methods can be adapted to IQ-SPECT to provide improved simultaneously acquired dual-radionuclide ^{99m}Tc/^{123}I cardiac images.

The simulation studies presented here demonstrate that the crosstalk from ^{123}I into the ^{99m}Tc energy window is largely due to downscatter. Therefore, it has broad spatial distribution and increased the image intensity of the entire ^{99m}Tc image, including the heart, blood pool, and other regions. The overall effect of this was reduced contrasts.

The crosstalk from ^{99m}Tc into the ^{123}I window was mainly from unscattered photons. Therefore its effects reflected the local distribution of the ^{99m}Tc: high in the normal regions and low in the regions with low uptake of the ^{99m}Tc agent. Similarly, in areas with normal ^{99m}Tc activity and reduced ^{123}I, corresponding to a denervated region with normal perfusion and thus a potential site for origin of arrhythmias, the contrast in the innervation image would be reduced. Even though the total crosstalk from ^{99m}Tc into the ^{123}I window was small, this localized effect can produce artifactual defects or obscure real ones, potentially leading to an incorrect diagnosis.

In this work both simulation and physical phantom studies have shown that the proposed model-based method provided accurate estimates of the crosstalk in both radionuclides' energy window. Compensation using the model-based method improved the simultaneous dual-radionuclide images so that they were comparable to single-radionuclide images.

Conclusions

We have developed a fast Monte Carlo simulation method and that accurately models the image formation process in a cardiac imaging system (IQ-SPECT) based on a novel multi-focal (SMARTZOOM) collimator. This simulation method has ben validated with physical phantom experiments. We then investigated the potential of IQ-SPECT using SMARTZOOM collimators to acquire simultaneous dual-radionuclide ^{99m}Tc perfusion/^{123}I innervation myocardial images. This system may be important for dual-radionuclide applications because of its potential to reduce patient dose. Using the simulation we evaluated the effects of crosstalk on simultaneously acquired images. In ^{99m}Tc images, the crosstalk from ^{123}I had a global effect due to the wide distribution of scattered photons. This resulted in a global increase in image intensity and thus a decrease in defect contrast. In ^{123}I images, the effects of ^{99m}Tc crosstalk were local and can produce artifactual defects or obscure real defects. A model-based method was developed to accurately model and compensation for the crosstalk contamination in the simultaneously acquired dual-radionuclide IQ-SPECT projection data. Validation using Monte Carlo simulation and physical phantom experiments demonstrated that the model-based method could provide accurate estimates of crosstalk contamination in both energy windows. Compensation using this model-based method greatly improved the dual-radionuclide images so that they were quantitatively and qualitatively comparable to single-radionuclide images.

Acknowledgments

The authors would like to thank Dr. Manjit Ray for making the IQ-SPECT projection operator available for this research. This work was supported by a research grant from Siemens Medical Solution Inc. and a Public Heath Service grant R01-EB00288.

References

Agostini D, Dronne F, Mulder P, Thulliez C, Bouvard G. Mismatch between cardiac neuronal and perfusion uptakes using a dual I-123-MIBG and Tl-201 kinetic study in rat with myocardial infarction. J Nucl Med. 2002; 43:172p.

Ben-Haim S, Kacperski K, Hain S, Van Gramberg D, Hutton BF, Erlandsson K, Sharir T, Roth N, Waddington WA, Berman DS, Ell PJ. Simultaneous dual-radionuclide myocardial perfusion imaging with a solid-state dedicated cardiac camera. European Journal of Nuclear Medicine and Molecular Imaging. 2010; 37:1710–21. [PubMed: 20383705]

Buvat I, Hapdey S, Benali H, Todd-Pokropek A, Di Paola R. Spectral factor analysis (SFA) for dual-isotope imaging. J Nucl Med. 1999; 40:116P–7P.

de Jong HWAM, Beekman FJ, Viergever MA, van Rijk PP. Simultaneous Tc-99m/Tl-201 dual-isotope SPET with Monte Carlo-based down-scatter correction. European Journal of Nuclear Medicine and Molecular Imaging. 2002; 29:1063–71. [PubMed: 12173021]

Devous MD, Lowe JL, Payne JK. Dual-Isotope Brain Spect Imaging with Technetium and I-123 - Validation by Phantom Studies. J Nucl Med. 1992; 33:2030–5. [PubMed: 1432168]

Du Y, Frey EC. Simultaneous (99m)Tc/(201)Tl/(123)I triple-isotope cardiac SPECT imaging. Ieee Nucl Sci Conf R. 2007:4213–6.

Du Y, Frey EC. Quantitative evaluation of simultaneous reconstruction with model-based crosstalk compensation for (99m)Tc/(123)I dual-isotope simultaneous acquisition brain SPECT. Med Phys. 2009; 36:2021–33. [PubMed: 19610291]

Du Y, Links JM, Becker L, DiPaula AF, Frank T, Schuleri KH, Lardo AC, Frey EC. Evaluation of simultaneous Tl-201/Tc-99m dual-isotope cardiac SPECT imaging with model-based crosstalk compensation using canine studies. J Nucl Cardiol. 2014; 21:329–40. [PubMed: 24366822]

Du Y, Tsui BMW, Frey EC. Model-based crosstalk compensation for simultaneous Tc-99m/I-123 dual-isotope brain SPECT imaging. Med Phys. 2007; 34:3530–43. [PubMed: 17926956]

El Fakhri G, Maksud P, Kijewski MF, Habert MO, Todd-Pokropek A, Aurengo A, Moore SC. Scatter and cross-talk corrections in simultaneous Tc-99m/I-123 brain SPECT using constrained factor analysis and artificial neural networks. Ieee T Nucl Sci. 2000; 47:1573–80.

Frey, EC.; Tsui, BMW. A new method for modeling the spatially-variant, object-dependent scatter response function in SPECT. 1996 IEEE Nuclear Science Symposium - Conference Record; 1997. p. 1082-6.

Fung GSK, Segars WP, Gullberg GT, Tsui BMW. Development of a model of the coronary arterial tree for the 4D XCAT phantom. Physics in Medicine and Biology. 2011; 56:5651–63. [PubMed: 21828911]

He X, Song XY, Frey EC. Application of Three-Class ROC Analysis to Task-Based Image Quality Assessment of Simultaneous Dual-Isotope Myocardial Perfusion SPECT (MPS). IEEE Transactions on Medical Imaging. 2008; 27:1556–67. [PubMed: 18955172]

Ivanovic M, Weber DA, Loncaric S, Franceschi D. Feasibility of Dual Radionuclide Brain Imaging with I-123 and Tc-99m. Med Phys. 1994; 21:667–74. [PubMed: 7935202]

Kadrmas DJ, Frey EC, Tsui BMW. Simultaneous technetium-99m/thallium-201 SPECT imaging with model-based compensation for cross-contaminating effects. Physics in Medicine and Biology. 1999; 44:1843–60. [PubMed: 10442716]

Milliner M, Burg S, Dieudonne A, Rouzet F, Hyafil F, Le Guludec D. Performances of cardiac dedicated D-SPECT camera for simultaneous dual isotope tomographic acquisitions: evaluation in phantoms. European Journal of Nuclear Medicine and Molecular Imaging. 2012; 39:S384–S5.

Miyamoto K, Nakata T, Yuda S, Uno K, Wakabayashi T, Tsuchihashi K, Shimamoto K. Mechanisms of impaired cardiac sympathetic innervation assessed by MIBG responsible for long-term cardiac death probability in patients with left ventricular dysfunction. Circulation. 1999; 100:310–1.

Moore SC, English RJ, Syravanh C, Tow DE, Zimmerman RE, Chan KH, Kijewski MF. Simultaneous Tc-99m/Tl-201 Imaging Using Energy-Based Estimation of the Spatial Distributions of Contaminant Photons. Ieee T Nucl Sci. 1995; 42:1189–95.

Ouyang J, El Fakhri G, Moore SC. Fast Monte Carlo based joint iterative reconstruction for simultaneous Tc-99m/I-123 SPECT imaging. Med Phys. 2007; 34:3263–72. [PubMed: 17879789]

Pace L, Betocchi S, Losi MA, Della Morte AM, Ciampi Q, Nugnez R, Chiariello M, Salvatore M. Sympathetic nervous function in patients with hypertrophic cardiomyopathy assessed by[I-123]-MIBG: relationship with left ventricular perfusion and function. Quarterly Journal of Nuclear Medicine and Molecular Imaging. 2004; 48:20–5. [PubMed: 15195000]

Pirich C, Keinrath P, Barth G, Rendl G, Krammel F, Rettenbacher L. Diagnostic Accuracy and Functional Parameters in Tc-99m tetrofosmine Myocardial Perfusion Scintigraphy using Accelerated Cardiac Aquisition with IQ SPECT Technique in Comparison to Conventional Imaging. European Journal of Nuclear Medicine and Molecular Imaging. 2012; 39:S285–S6.

Harrison RLSBG, Vannoy SD, Kaplan MS, Lewellen TK. A public domain simulation system for emission tomography: photon tracking through heterogeneous attenuation using importance sampling. J Nucl Med. 1993; 34:60P.

Harrison, RL.; Haynor, SDVDR.; Gillispie, SB.; Kaplan, MS.; Lewellen, TK. Preliminary Experience with the Photon History Generator Module of a Public-Domain Simulation Systems for Emission Topography. IEEE Nuc. Sci. Symp. and Med. Im. Conf; 1994.

Raffel DM, Wieland DM. Development of mIBG as a Cardiac Innervation Imaging Agent. Jacc-Cardiovascular Imaging. 2010; 3:111–6. [PubMed: 20129540]

Rajaram, R.; Bhattacharya, M.; Ding, XH.; Malmin, R.; Rempel, TD.; Vija, AH.; Zeintl, J. Tomographic Performance Characteristics of the IQ.SPECT System. 2011 IEEE Nuclear Science Symposium and Medical Imaging Conference (Nss/Mic); 2011. p. 2451-6.

Sakata K, Iida K, Mochizuki N, Ito M, Nakaya Y. Physiological Changes in Human Cardiac Sympathetic Innervation and Activity Assessed by I-123-Metaiodobenzylguanidine (MIBG) Imaging. Circulation Journal. 2009; 73:310–5. [PubMed: 19057084]

Schillaci O, Danieli R. Dedicated cardiac cameras: a new option for nuclear myocardial perfusion imaging. European Journal of Nuclear Medicine and Molecular Imaging. 2010; 37:1706–9. [PubMed: 20593283]

Song X, Frey EC, Wang WT, Du Y, Tsui BMW. Validation and evaluation of model-based crosstalk compensation method in simultaneous Tc-99m stress and Tl-201 rest myocardial perfusion SPECT. Ieee T Nucl Sci. 2004; 51:72–9.

Song X, Segars WP, Du Y, Tsui BMW, Frey EC. Fast modelling of the collimator-detector response in Monte Carlo simulation of SPECT imaging using the angular response function. Phys Med Biol. 2005; 50:1791–804. [PubMed: 15815096]

Yukinaka M, Nomura M, Ito S, Nakaya Y. Mismatch between myocardial accumulation of I-123-MIBG and Tc-99m-MIBI and late ventricular potentials in patients after myocardial infarction: Association with the development of ventricular arrhythmias. Am Heart J. 1998; 136:859–67. [PubMed: 9812082]

Zaret, BL.; Beller, GA. Clinical Nuclear Cardiology: state of the art and future directions. 4. Vol. 41. Mosby Elsevier; 2010a. p. 657-73.

Zaret, BL.; Beller, GA. Clinical Nuclear Cardiology: state of the art and future directions. 4. Vol. Charpters 14 and 15. Mosby Elsevier; 2010b. p. 225-86.

Zhao C, Shuke N, Yamamoto W, Okizaki A, Sato J, Ishikawa Y, Ohta T, Hasebe N, Kikuchi K, Aburano T. Comparison of cardiac sympathetic nervous function with left ventricular function and perfusion in cardiomyopathies by I-123-MIBG SPECT and Tc-99m-tetrofosmin electrocardiographically gated SPECT. J Nucl Med. 2001; 42:1017–24. [PubMed: 11438621]

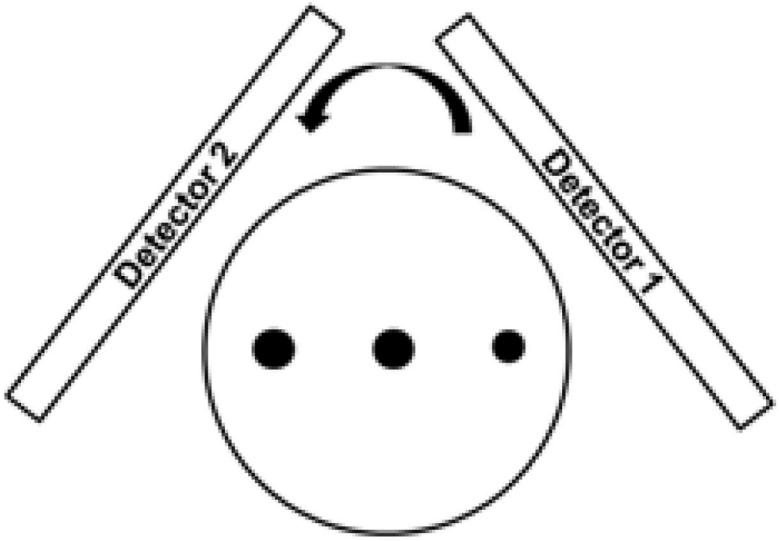

Figure 1.
Phantom used for validating SimSET-ARF Monte Carlo simulation

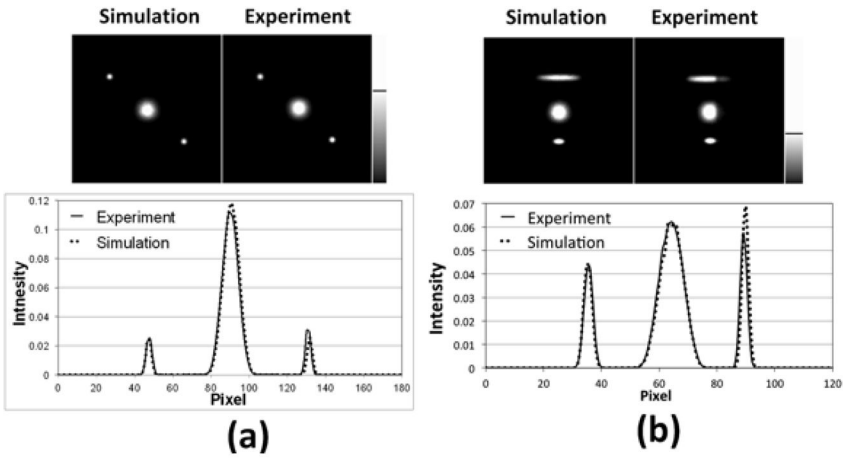

Figure 2.

Simulated and experimentally acquired projections of three spheres in air at: a) parallel view; b) perpendicular view. Profiles across the center of the spheres are also shown below the images. Note that the gray scale was windowed to amplify the lower-count regions.

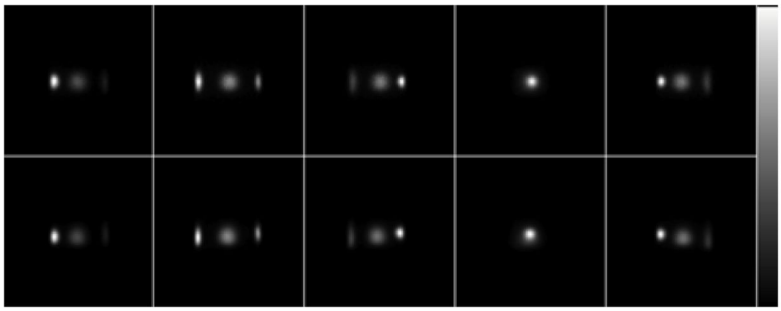

Figure 3.
Simulated and experimentally acquired projections of three spheres in a water filled cylinder. Top row: ARF simulated results; bottom row: experimentally acquired results.

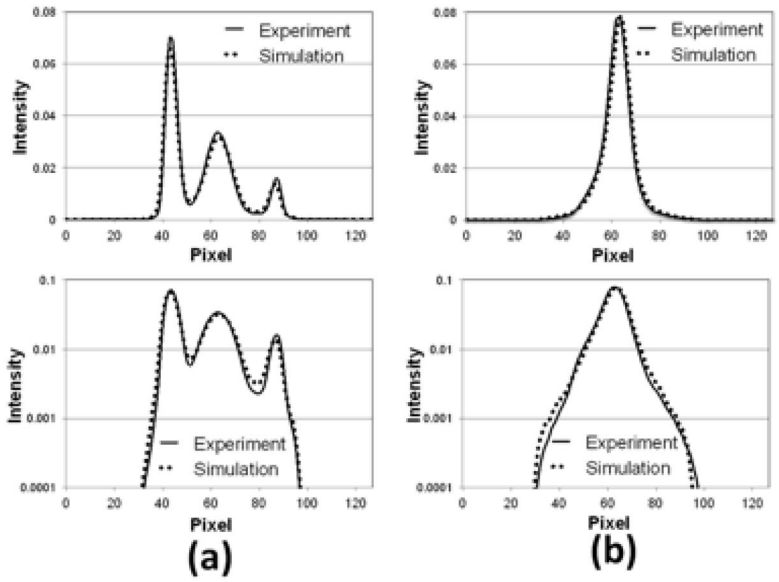

Figure 4.

Horizontal profiles of the simulated and experimentally acquired projections shown in Figure 3. a), profiles of the first projection from the left; b), profiles of the fourth projection from the left. The profiles are plotted in both linear scale (top) and logarithmic scale (bottom).

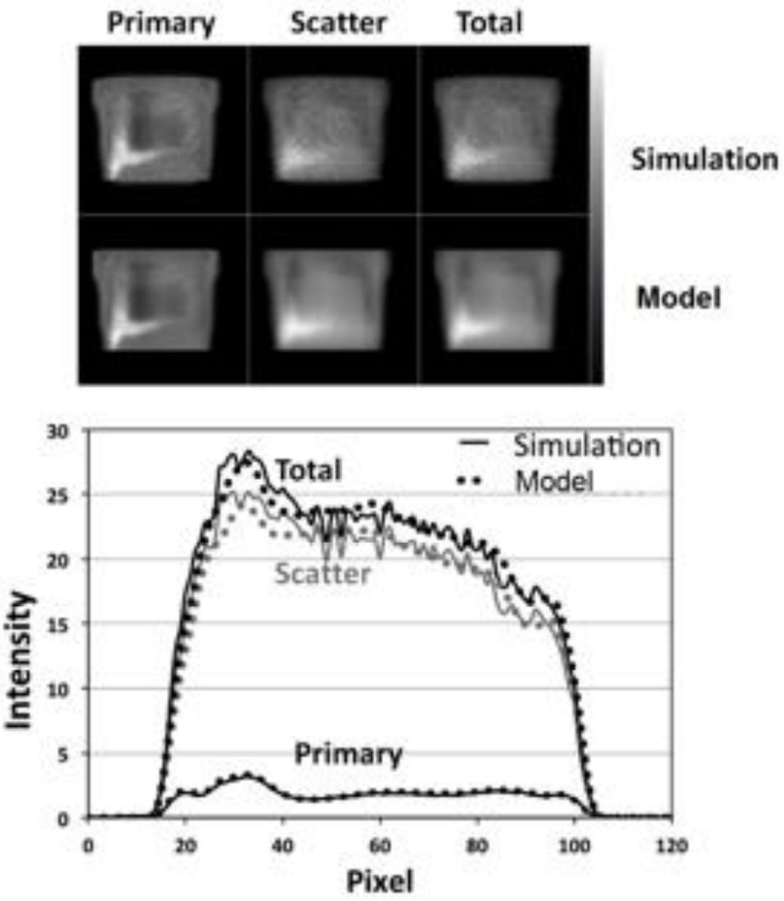

Figure 5.

Comparison of model-base estimated crosstalk from ^{123}I into the ^{99m}Tc energy window with simulated result at anterior view. Horizontal profiles across the heart region are also plotted. Primary: unscattered photons; Scatter: photons scattered inside object; Total: sum of primary and scatter photons.

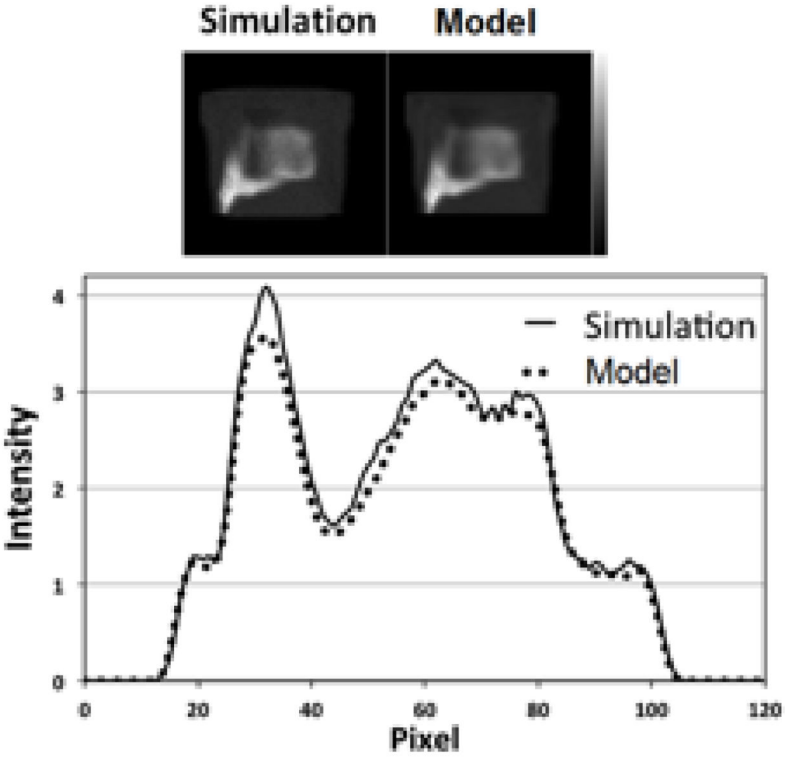

Figure 6.

Comparison of model-base estimated crosstalk from ^{99m}Tc into the ^{123}I energy window with simulated result at anterior view. Horizontal profiles across the heart region are also plotted.

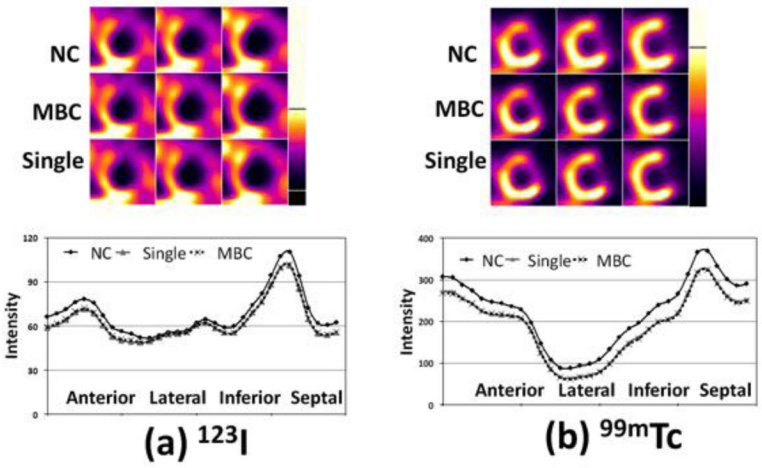

Figure 7.

Short axis images and circumferential profiles from the ^{123}I and ^{99m}Tc images from the simulation validation. NC: images with crosstalk contamination but without crosstalk compensation; MBC: images with crosstalk contamination and model-based crosstalk compensation; Single: single-radionuclide images without crosstalk contamination.

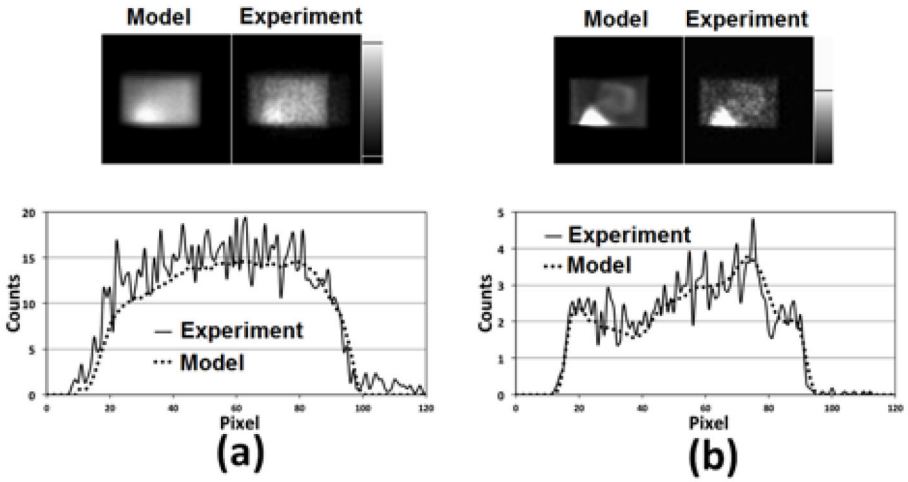

Figure 8.

Comparison of model-based estimates of the crosstalk with measured data for the 45° right anterior oblique view from the physical phantom experiment. Horizontal profiles through the heart region are shown at the bottom. a) crosstalk from ^{123}I into the ^{99m}Tc energy window and b) crosstalk from ^{99m}Tc into the ^{123}I energy window.

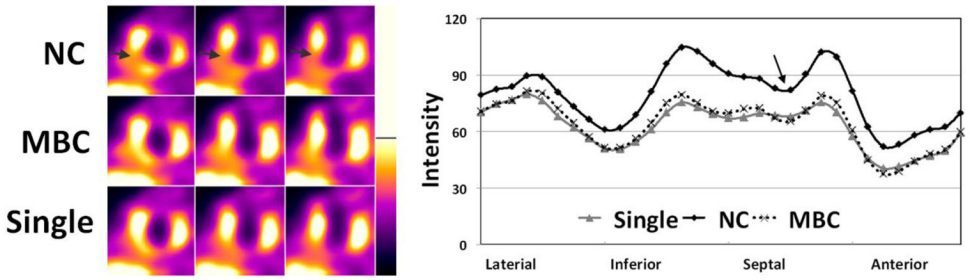

Figure 9.

Short axis ^{123}I images and their circumferential profiles from physical phantom experiment. NC: images with crosstalk contamination but without crosstalk compensation; MBC: images with crosstalk contamination and model-based crosstalk compensation; Single: single-radionuclide images without crosstalk contamination. The arrows point to the location of artifactual defect caused by crosstalk.

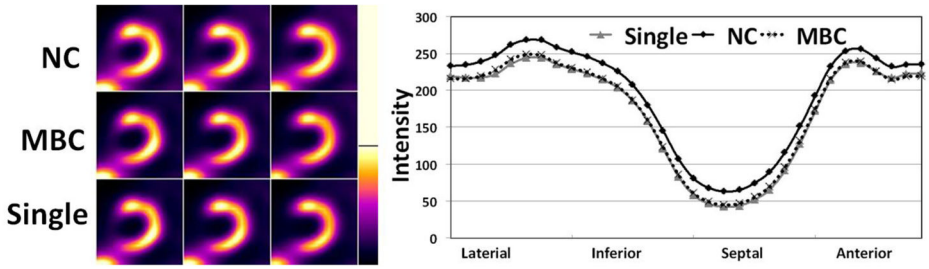

Figure 10.

Short axis ^{99m}Tc images and their circumferential profiles from physical phantom experiment. NC: images with crosstalk contamination but without crosstalk compensation; MBC: images with crosstalk contamination and model-based crosstalk compensation; Single: single-radionuclide images without crosstalk contamination.

Table 1

Activity concentration in the XCAT phantom (arbitrary unit).

	I-123	Tc99m	Tc/I ratio
Background	13.2	10	0.76
Liver	31.6	60	1.90
Heart	26.4	100	3.79
Blood Pool	2.64	10	3.79
Lung	7.94	5	0.63
Defect	7.94	10	1.26

Table 2

Activity concentrations filled in the physical phantom.

	^{123}I (uCi/cc)	^{99m}Tc (uCi/cc)	^{99m}Tc/^{123}I ratio
Background	0.681	0.978	1.436
Liver	1.727	6.116	3.541
Heart	2.713	7.992	2.946